

The Carina Dwarf Spheroidal Galaxy: A Goldmine for Cosmology and Stellar Astrophysics

Peter B. Stetson¹
 Matteo Monelli^{2, 3}
 Michele Fabrizio⁴
 Alistair Walker⁵
 Giuseppe Bono^{4, 6, 7}
 Roberto Buonanno^{4, 8}
 Filippina Caputo⁶
 Santi Cassisi⁹
 Carlo Corsi⁶
 Massimo Dall’Ora¹⁰
 Scilla Degl’Innocenti^{11, 12}
 Patrick François¹³
 Ivan Ferraro⁶
 Roberto Gilmozzi⁷
 Giacinto Iannicola⁶
 Thibault Merle¹⁴
 Mario Nonino¹⁵
 Adriano Pietrinferni⁹
 Pier Prada Moroni^{11, 12}
 Luigi Pulone⁶
 Martino Romaniello⁷
 Frederic Thévenin¹⁴

¹ DAO/HIA/NRC, Victoria, Canada

² IAC, Tenerife, Spain

³ Univ. La Laguna, Tenerife, Spain

⁴ Univ. Tor Vergata, Roma, Italy

⁵ NOAO/CTIO, La Serena, Chile

⁶ INAF–OAR, Monte Porzio Catone, Italy

⁷ ESO

⁸ ASDC, Frascati, Italy

⁹ INAF–OACTe, Teramo, Italy

¹⁰ INAF–OAC, Napoli, Italy

¹¹ Univ. Pisa, Pisa, Italy

¹² INFN, Pisa, Italy

¹³ Obs. de Paris-Meudon, Paris, France

¹⁴ Obs. Côte d’Azur, Nice, France

¹⁵ INAF–OAT, Trieste, Italy

We present deep and precise multiband (U , B , V , I) optical data for the Carina dwarf spheroidal galaxy. Data were collected using three different ground-based telescopes (4-metre Blanco CTIO, MPG/ESO 2.2-metre, 1.5-metre CTIO) and cover the entire body of the galaxy. We discuss the reliability of the absolute photometric zero-point calibrations of images collected with large-format and mosaic CCD cameras. The typical precision for the B -, V - and I -bands is better than 0.01 mag. The U -band is a little worse. A preliminary comparison with scaled-solar and α -enhanced evolutionary predictions covering a broad range of ages and chemical compositions seems to

support previous photometric evidence that both the old (12 Gyr) and the intermediate-age (4–6 Gyr) subpopulations show a limited spread in chemical composition. The use of the Carina galaxy field as a possible standard stellar field is outlined.

Introduction

Dwarf galaxies play a fundamental role in several astrophysical problems. Current cosmological simulations predict dwarf satellite populations significantly larger than the number of dwarfs observed near giant spirals like the Milky Way and M31. This discrepancy is known as the missing satellite problem and challenges the current most popular cosmological model: the Lambda Cold Dark Matter paradigm (Madau et al., 2008). However, it is not yet known whether this discrepancy is due to limitations in the theoretical modelling or to observational bias at the faint end of the galaxy luminosity function (Kravtsov, 2010).

The distribution of dwarf galaxies in multi-dimensional parameter space indicates that they follow very tight relations. In particular, Prada & Burkert (2002) suggested that Local Group (LG) dwarf galaxies show strong correlations (Fundamental Line [FL]) between mass-to-light (M/L) ratio, surface brightness and metallicity (Z). They explained the correlation between M/L ratio and Z using a simple chemical enrichment model where the hot metal-enriched gas, at the end of the star formation epoch, is lost via galactic winds (Mac Low & Ferrara, 1999; Woo et al., 2008). Furthermore, the FL of dwarf irregulars (dIs) in a five-dimensional parameter space (total mass, surface brightness, rotation velocity, metallicity and star formation rate) is linear and tight, and extends the scaling relations of giant late-type galaxies to lower mass. On the other hand, the FL of dwarf spheroidals (dSphs) in a four-dimensional parameter space (total mass, surface brightness, rotation velocity and Z) is also linear and very tight, but is not an extrapolation of the scaling relations of giant early-type galaxies.

Carina plays a key role among the LG dSph galaxies for many reasons:

- i) it is relatively close, and its central density is modest;
- ii) it shows multiple star formation episodes, separated in time and in the amount of stellar mass involved (Monelli et al., 2003);
- iii) it hosts a broad variety of variable stars ranging from low- and intermediate-mass hydrogen-burning dwarf Cepheids to low- and intermediate-mass helium-burning stars (Anomalous Cepheids; Dall’Ora et al., 2003);
- iv) high resolution spectra are available for fewer than a dozen bright red giants (RGs). The mean metallicity is $[Fe/H] = -1.69$ with a spread of 0.5 (Koch et al., 2008);
- v) calcium triplet measurements based on medium resolution spectra are also available for a large sample (437) of RG stars (Koch et al., 2006) with a peak at $[Fe/H] = -1.72$, but ranges from -2.5 to -0.5 . Using the same spectra, but different selection criteria, Helmi et al. (2006) found a metallicity distribution from about -2.3 to -1.3 .

However, we are facing a stark discrepancy between the spread in metallicity suggested by spectroscopic measurements and photometric metallicity indicators. Deep and accurate colour–magnitude diagrams (CMDs) of Carina indicate that the width in colour of the red giant branch (RGB) is quite limited (Monelli et al., 2003; Harbeck et al., 2001). This evidence was further supported in a recent investigation by Bono et al. (2010) employing a large number of multiband (U , B , V , I) CCD images from ground-based telescopes covering the entire body of the galaxy.

Photometric datasets and photometric calibration

The data were collected in various observing runs between December 1992 and January 2005. They include images from three telescopes: the Cerro Tololo Inter-American Observatory (CTIO) 1.5-metre telescope with a single Tektronix 2K CCD, the CTIO 4-metre Blanco telescope with the Mosaic II camera, and the MPG/ESO 2.2-metre telescope with the Wide Field Imager (WFI) camera (both

proprietary and archival data). The data discussed here represent 4152 individual CCD images with essentially complete coverage of the central regions of Carina (about 40 by 55 arcminutes, lacking only those regions obliterated by bright foreground stars). They were obtained in four photometric bands (B and I with the 1.5-metre telescope, and $UBVI$ with both the 4-metre and 2.2-metre telescopes). The resulting colour image is shown on p. 20.

The photometric data were reduced using the DAOPHOT/ALLFRAME package (Stetson, 1987; 1994). Because of the multiple chips and pointings, any given star may have up to 17 calibrated measurements in U , 156 in B , 207 in V , and 70 in I . A total of 205 338 individual stars were catalogued and measured. Among these, 72 595 have photometric measurements in all four filters, while 129 230 have at least V and either $B-V$ or $V-I$. The remainder, either extremely faint (*i.e.*, detectable in only one filter) or located near the periphery, have astrometry and instrumental magnitudes only.

The fundamental standard system of photometric magnitudes was established decades ago using photoelectric photometers on small telescopes — mostly of apertures 0.4–0.9 metres (e.g., Landolt, 1973; 1988; 1992; Graham, 1982; and references therein to the establishment of UBV by Johnson and RI by Cousins). One of the authors (PBS) has spent a sig-

nificant part of his career attempting to ensure that measurements of very faint stars obtained with CCDs on large telescopes are on the same photometric system as measurements of very bright stars made with photomultipliers on small telescopes (Stetson, 2000; 2005)¹.

The question of whether the photometry discussed here is on the standard system breaks down into two parts:

- i) the extent to which the CCD photometry, in general, is on the standard system; and
- ii) the extent to which the photometry for Carina, in particular, is on the same system as the rest of the photometry. As of now, 2076 datasets have been homogeneously analysed through our software; among these, 1591 are considered to be of photometric quality, and 485 have been analysed in non-photometric mode (*viz.* data taken under non-photometric conditions).

Figure 1 shows the magnitude differences between the calibrated standard-system magnitudes from our own observations of the fundamental photometric standards, as compared to the published values for the same stars. In order to restrict the comparison to stars with the most reliable data, we consider only magnitudes based on at least five independent measurements obtained on photometric occasions, and having standard errors of the mean not greater than 0.02 mag based on the internal

repeatability of the observations. For our measurements we were able to impose the additional condition that each star shows no evidence of intrinsic variation at a level greater than 0.05 mag root mean square (rms), when the data from all filters are considered.

The left panels of Figure 1 show the magnitude residuals (in the sense *published* minus *ours*) plotted versus apparent visual magnitude, while the right panels of Figure 1 plot the same residuals against the $B-I$ colour. The differences show a systematic departure of a few hundredths of a magnitude between our photometric system and the standard system for stars brighter than approximately $V = 9$. We infer that the stars with $V \leq 9$ were simply too bright to be measured with our equipment, and we were unduly optimistic about these measurements. We therefore advise readers to ignore Stetson's results for standard stars with $V \leq 9$ and rely entirely upon the previously published photometric indices of such stars instead. Figure 1 demonstrates that our photometry matches the definitive published results with a high degree of fidelity over a dynamic range of ~ 600 in flux ($9 \leq V \leq 16$) and over the full available range of stellar temperature. Quantitatively, the weighted mean differences between the published results and ours are $+0.0012 \pm 0.0028$, $+0.0016 \pm 0.0013$, -0.0007 ± 0.0009 and -0.0025 ± 0.0013 mag in U , B , V and I , respectively, based upon 109, 209, 220 and

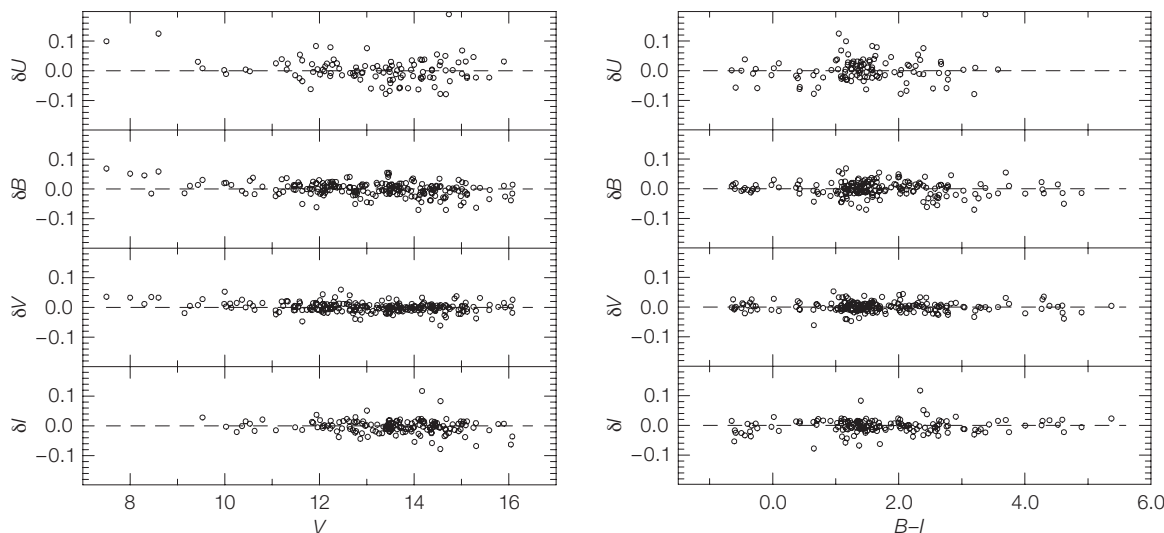


Figure 1. Left: From top to bottom, difference in U -, B -, V - and I -bands between standard system magnitudes and the current observations of the fundamental photometric standards as a function of the visual magnitude. Right: Same as the left, but the difference in magnitude is plotted as a function of $B-I$.

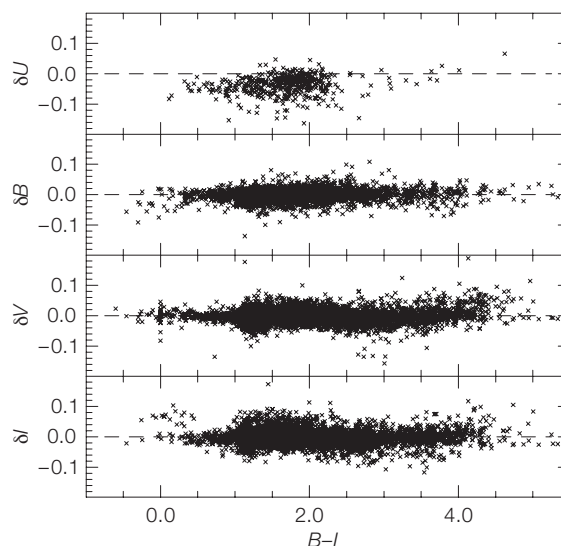
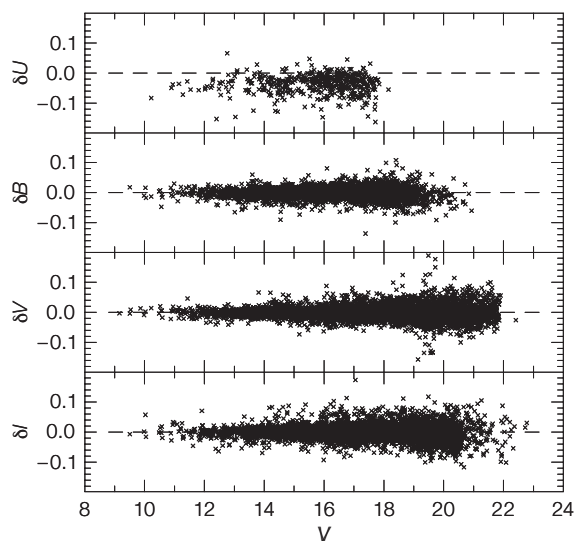


Figure 2. Left: Same as the left panels of Figure 1, but the difference is between magnitudes based on datasets from nights when Carina was observed (175 photometric, 88 non-photometric) as compared to results from the rest of our nights — when Carina was not observed (1416 clear, 397 cloudy) — for those stars in all our other fields that appear in both datasets. See text for more details. Right: Same as left, but difference in magnitude is plotted as a function of $B-I$.

151 stars. Expressed as a standard deviation, the average standard residual of one star is 0.027, 0.017, 0.012, 0.012 and 0.016 mag in U , B , V , R and I . It does not seem that these numbers can be reduced by obtaining more observations; rather, they represent a fundamental limit to the reliability with which any given *individual* star can be referred to a fundamental standard system, due to the fact that even though stars may have the same broadband colours in one photometric system, they can still have underlying spectral energy distributions that differ in detail, and that will be sampled differently by other filter sets.

Figure 2 provides the same sort of comparison for all stars in all fields in the Carina observations (263 in number: 175 photometric, 88 non-photometric) as compared to results for the same target stars appearing in our 1813 datasets obtained on nights when Carina was *not* observed (1416 clear, 397 cloudy). Again we have restricted the comparison to stars with at least five photometric observations, standard errors no larger than 0.02 mag and no evidence of intrinsic variation in excess of 0.05 mag rms when data from all filters are considered. These new comparisons show a few significant photometric outliers with magnitude differences > 0.10 mag, as expected in any large body of raw data, but the vast majority of stars show that the datasets that do include Carina observations are reasonably well matched to the rest of

our CCD data *except* in the U filter. In this filter only, 451 stars common to the two samples — all of which lie in *only one* field, Selected Area 98 — show a systematic offset of 0.036 mag.

The Johnson U bandpass has always been a little problematic. Its classical implementation provided a bandpass defined by filter throughput on the long wavelength side, but by atmospheric opacity on the short wavelength side. Furthermore, the atmospheric extinction in the U -band is very high: ~ 0.5 mag per airmass on *good* nights at 2000 metres on mountaintops like Cerro Tololo or La Silla. Finally, this bandpass contains the Balmer convergence and jump in hot stars, and a multitude of strong metal lines (including Ca II H+K) and bands of molecules like CN in cool stars. All of these features make the U magnitudes sensitive to the exact placement and shape of the instrumental bandpass. We will continue to investigate the cause of this discrepancy, but for the present we expect that a correction of order one-tenth to one-half the difference should be applied to our U -band results for Carina to bring them closer to the standard system.

The problem is that we do not have many *other* nights of southern hemisphere observations that included measurements in the U -band, to which we could compare. Quantitatively, apart from U , the formal weighted mean magni-

tude differences are +0.0010, -0.0002 , -0.0001 mag in B , V and I , respectively, based on 8795, 14945, and 10329 stars. The formal statistical confidence intervals on these numbers are all $< 1 \times 10^{-4}$ mag, but these are certainly underestimated; we still need to think harder about how to characterise our actual systematic uncertainties, given that so few independent points of comparison are available to us. However, the current evidence suggests that systematic differences between our Carina observations and the system of Landolt and Graham in B , V and I probably do not greatly exceed a few times 0.001 mag, and calibration issues will not be a significant limiting factor for our interpretations so long as we use U only for differential comparisons within our data.

Comparison between theory and observations

A detailed comparison between stellar populations in Carina with simple stellar populations belonging either to Galactic globular clusters (GCs) or to intermediate-age clusters in the Small Magellanic Cloud was presented in Bono et al. (2010). The discrimination between field and Carina stars was performed using the $U-V$, $B-I$ colour-colour plane. Figure 3 shows three different CMDs of the candidate Carina stars. Note that after the selection there remain some field stars with colours similar to Carina's RGB

($V \leq 21.5$, $B-V \sim 0.5$ mag). The evolutionary properties of low- and intermediate-mass stars provide at least three independent metallicity indicators: the slope and the spread in colour of RGB stars; the spread in colour of red clump (RC) stars; and the spread in magnitude of blue and red horizontal branch (HB) stars. Data plotted in this figure show that both RGB and RC stars cover a very limited range in colour in the three adopted CMDs. The same observation applies to the spread in magnitude of blue and red HB stars.

The theoretical framework for both scaled-solar and α -enhanced evolutionary models is based on isochrones available in the BaSTI database (Pietrinferni et al., 2004; 2006). To compare theory and observations we adopted the distance modulus and the reddening available in the literature (Dall’Ora et al., 2003; Monelli et al., 2003). As a first working hypothesis, we are assuming that both the old and the intermediate-age subpopulations have scaled-solar chemical compositions. Spectroscopic investigations indicate that α -elements in dSph galaxies may be overabundant when compared with solar composition, but underabundant when compared with GCs of similar metallicity (Tolstoy et al., 2009; and references therein).

The left panels of Figure 4 show the comparison in the V , $B-V$ CMD, at fixed chemical composition ($[Fe/H] = -1.79$, $Y = 0.245$), with two old (top; 10, 12 Gyr) and three intermediate-age (bottom; 2, 4, 6 Gyr) isochrones. Data plotted in these panels display that theory and observations, within the errors, agree quite well. The intermediate-age isochrones appear slightly bluer than the bulk of the RGB stars, but the difference is of the order of a few hundredths of a magnitude. The right panels of Figure 4 show the comparison at fixed age and different chemical compositions. In particular, the top right panel shows the comparison with three old isochrones of 12 Gyr and iron abundances ranging from -2.3 to -1.5 dex. Note that evolutionary models were constructed assuming a helium-to-metal enrichment ratio $\Delta Y/\Delta Z = 1.4$ and a mass-loss rate $\eta = 0.4$ (Pietrinferni et al., 2004). The colour range covered by the

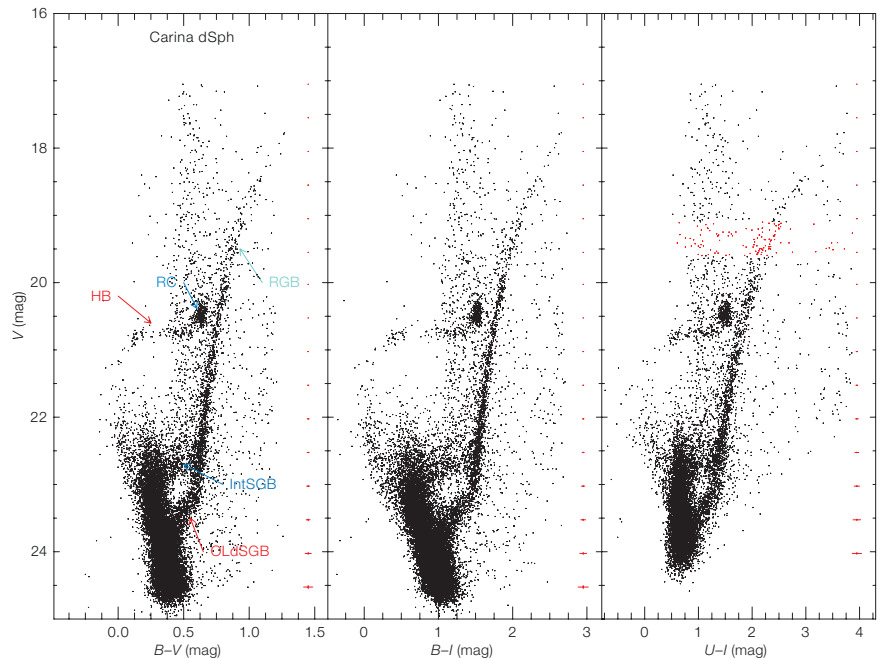


Figure 3. Left: $B-V$, V colour-magnitude diagram of candidate Carina stars based on optical images collected with the MOSAIC camera at the 4-metre Blanco telescope, with the WFI at the MPG/ESO 2.2-metre telescope and with the 1.5-metre CTIO telescope. The blue labels mark intermediate-age stellar tracers (SGB, RC), while the red ones the old

stellar tracers (SGB, HB). The red bars plotted at the right display the intrinsic photometric error both in magnitude and in colour. Middle: Same as left, but candidate Carina stars are plotted in the $B-I$, V colour-magnitude diagram. Right: Same as left, but candidate Carina stars are plotted in the $U-I$, V colour-magnitude diagram.

isochrones is systematically larger than observed over the magnitude range of sub-giant branch (SGB) and RGB stars. The same outcome applies to the intermediate-age (6 Gyr) subpopulation. The current predictions with the most metal-poor composition attain colours that are similar to the red tail of RC stars. However, the observed CMDs show a well defined separation between RC and RGB stars.

To further constrain the impact of chemical composition on the evolutionary properties of Carina stellar populations, we assumed that both the old and the intermediate-age sub-populations are α -enhanced. The left panels of Figure 5 show the comparison with two old (top; 10, 12 Gyr) and three intermediate-age (bottom; 2, 4, 6 Gyr) isochrones constructed assuming the same iron content as the scaled-solar isochrones adopted in Figure 4, but an overabundance of α -elements: $[\alpha/Fe] = 0.4$. The comparison between theory and observation appears slightly better than for the scaled-solar isochrones, since both

the old and the intermediate-age predictions attain colours that are similar to the observed ones. In addition, we repeated the comparison using isochrones assuming different values of global metallicity ($[M/H]$, see labelled values). The right panels of Figure 5 show the comparison with isochrones of 12 Gyr (top) for the old and of 6 Gyr for the intermediate-age sub-population.

The key advantage in the approach we adopted to compare theory and observations is that we are using theoretical predictions to constrain the *relative* difference and the *spread* in the heavy element abundances of Carina subpopulations. The above findings indicate that the possible abundance spreads of both the old and the intermediate-age subpopulations appear to be limited and of the order of 0.2–0.3 dex (Bono et al., 2010; Fabrizio et al., 2011), thus supporting the spread in iron abundances based on high resolution spectra provided by Shetrone et al. (2003). Theoretical and empirical uncertainties do not allow us to reach firm conclusions regarding

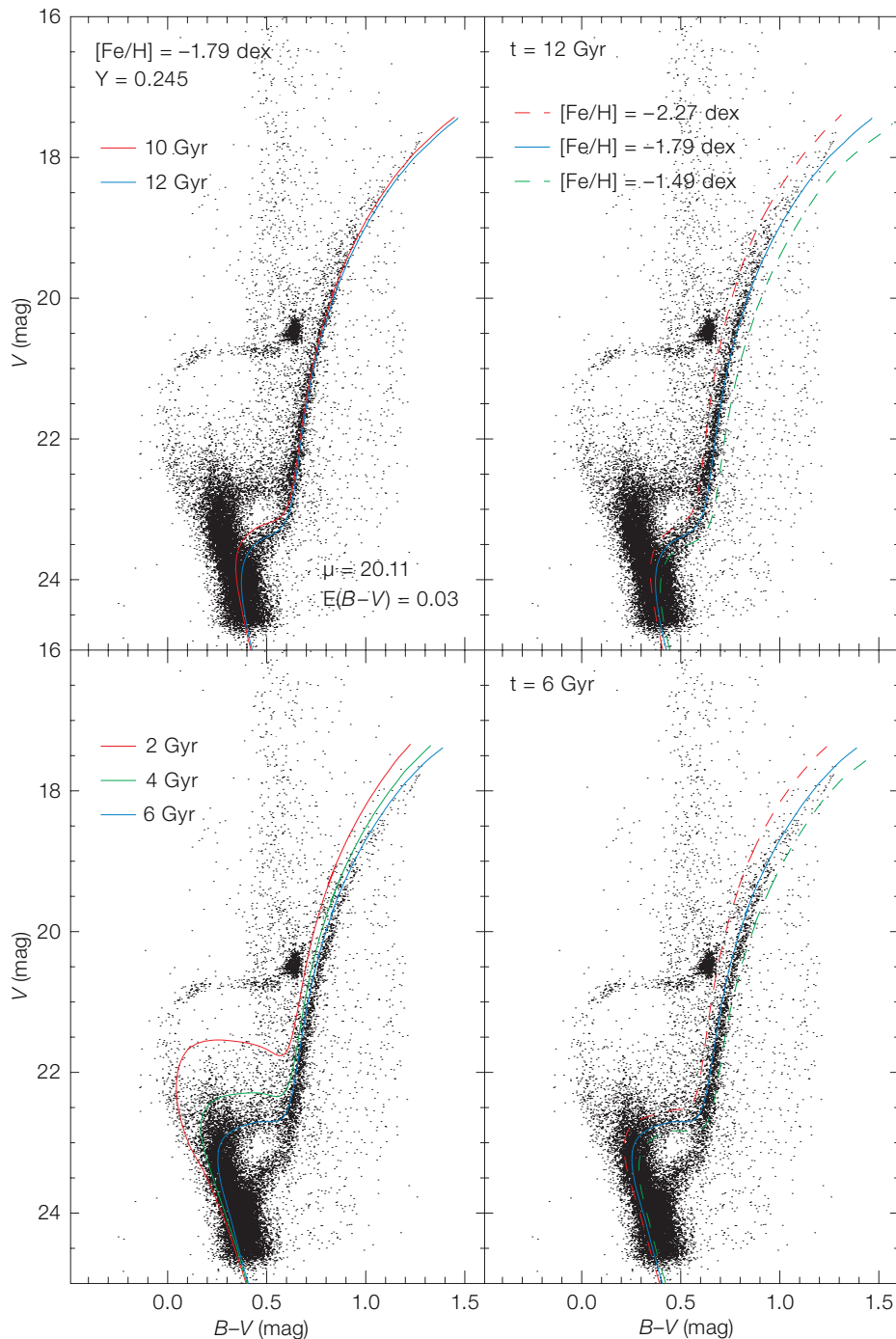


Figure 4. Left: $B-V$, V colour–magnitude diagram of Carina based on optical images. The solid coloured lines display two old (top) and three intermediate-age (bottom) scaled-solar isochrones at fixed iron abundance and different ages. The adopted true distance modulus and the reddening are also indicated. Right: Same as left panels, but comparison assumed an age of 12 Gyr for the old (top) and of 6 Gyr for the intermediate-age (bottom) subpopulation.

the possible occurrence of an α -element enhancement.

Future prospects

The identification of the physical mechanisms that drive the formation and the evolution of stars and stellar systems,

and the interplay between Big Bang nucleosynthesis and the creation of chemical elements in stars is one of the landmark achievements in astrophysics. The former largely relies on photometry, the latter on spectroscopy. Many of the current open problems in stellar astrophysics are approached through a comparison between the theoretical and observational Hertzsprung–Russell diagrams. This comparison relies on three fundamental pillars: absolute distances, photometric calibrations, and input physics adopted in the stellar evolutionary and pulsation models.

There is a threefold motivation for the ongoing effort for precise photometric calibrations for stellar populations in nearby dwarf galaxies:

- i) A systematic drift in photometric precision when moving from bright to faint RG stars might produce a spread in colour, and in turn, mimic a spread in metal content. Moreover, these systems are characterised by very low stellar densities, thus requiring that photometry be collected with large format and mosaic CCD cameras. Intense effort to achieve consistent zero-points across the field is mandatory to avoid spurious broadening of the key evolutionary sequences.
- ii) Dwarf galaxies in the Local Group and in the local volume are often contaminated by foreground field stars. Their colours, unfortunately, are similar to the colours of Galactic RGs and main sequence (MS) stars, once again mimicking a broadening in colour due to a spread in age and/or in metallicity. The separation of field and Galactic stars can be performed using radial velocity and/or proper motions, but at present this approach is limited to relatively bright RGs. A robust cleaning of MS and SG sequences can be performed using colour–colour planes (Bono et al., 2010) and/or a statistical subtraction of a control field (Balbinot et al., 2010). These approaches require, once again, very precise calibration in different bands across multiple telescope pointings.
- iii) The use of variable stars as distance indicators, stellar tracers and physics laboratories requires precise time series data and multiband calibrations.

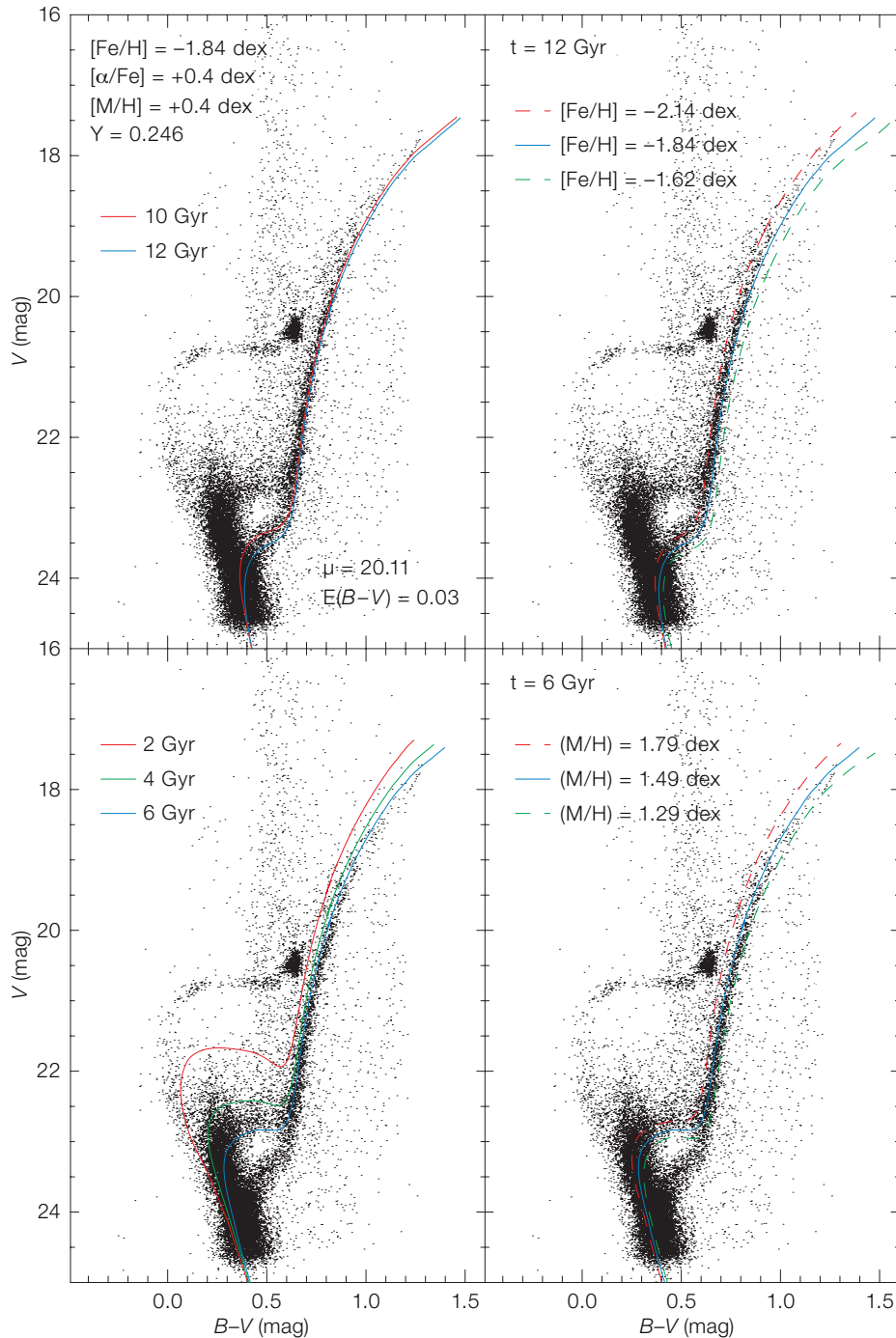


Figure 5. Left: Same as left panels of Figure 4, but comparison performed using isochrones constructed by assuming the same iron content ($[\text{Fe}/\text{H}] = -1.84$ dex) of the scaled-solar models, but with an α -enhanced chemical composition (see labelled values). Right: Same as left panels, but comparison performed using isochrones with different global metallicities ($[\text{M}/\text{H}]$, see labelled values).

The way to easily overcome the above problems is to have a sizable sample of local standard stars covering a broad range of magnitudes and colours. Local standards are now available in a significant fraction of globular clusters. So far, only a few dwarf galaxies have precise local standard stars in the optical

and in near-infrared (NIR) bands. All three Carina fields have 659 U -band, 5711 B - and V -band and 1467 I -band standard stars spanning a region 123 by 149 arc-minutes. The brightest standard has $V = 13.95$; the median is $V = 19.27$; and the faintest $V = 22.42$ mag. The Carina region together with other regions¹ is thus a potential standard stellar field to calibrate the next generation of large CCD cameras.

The use of accurate and deep NIR data, together with the present dataset, can play a crucial role in the identification of field and Carina candidate stars using optical–NIR colour–colour planes. The stronger sensitivity to effective temperature of the optical–NIR colours can also provide a robust separation between old and intermediate-age stars. At the same time, a high-resolution, high signal-to-noise ratio spectroscopic study of a sizable sample of RG stars and He-burning (RC, HB) stars is mandatory to *measure* the abundance spread, if any, in old and intermediate-age stellar populations.

References

- Balbinot, E. et al. 2010, MNRAS, 404, 1625
 Bono, G. et al. 2010, PASP, 122, 651
 Dall’Ora, M. et al. 2003, AJ, 126, 197
 Fabrizio, M. et al. 2011, PASP accepted
 Graham, J. A. 1982, PASP, 94, 244
 Helmi, A. et al. 2006, ApJL, 651, L121
 Koch, A. et al. 2006, AJ, 131, 895
 Koch, A. et al. 2008, AJ, 135, 1580
 Kravtsov, A. 2010, Advances in Astronomy, 2010,
 Landolt, A. U. 1973, AJ, 78, 959
 Landolt, A. U. 1983, AJ, 88, 439
 Landolt, A. U. 1992, AJ, 104, 340
 Mac Low, M. & Ferrara, A. 1999, ApJ, 513, 142
 Madau, P. et al. 2008, ApJ, 679, 1260
 Monelli, M. et al. 2003, AJ, 126, 218
 Pietrinferni, A. et al. 2004, ApJ, 612, 168
 Pietrinferni, A. et al. 2006, ApJ, 642, 797
 Prada, F. & Burkert, A. 2002, ApJ, 564L, 73
 Shetrone M. D., et al. 2003, AJ, 125, 684
 Stetson, P. B. 1987, PASP, 99, 191
 Stetson, P. B. 1994, PASP, 106, 250
 Stetson, P. B. 2000, PASP, 112, 925
 Stetson, P. B. 2005, PASP, 117, 563
 Tolstoy, E., Hill, V. & Tosi, M. 2009, ARA&A, 47, 371
 Woo, J., Courteau, S. & Dekel, A. 2008, MNRAS, 390, 1453

Links

¹ List of photometric standard fields: <http://www3.cadc-ccda.hia-ihp.nrc-cnrc.gc.ca/community/STETSON/standards/>